Am J Physiol Gastrointest Liver Physiol 308: G251–G261, 2015.
First published December 11, 2014; doi:10.1152/ajpgi.00137.2014.

A high-fat diet modulates iron metabolism but does not promote liver fibrosis in hemochromatotic Hjv$^{-/-}$ mice

Ranjit Singh Padda,[1] Konstantinos Gkouvatsos,[1] Maria Guido,[2] Jeannie Mui,[3] Hojatollah Vali,[3] and Kostas Pantopoulos[1]

[1]*Lady Davis Institute for Medical Research, Jewish General Hospital, and Department of Medicine, McGill University, Montreal, Quebec, Canada;* [2]*Department of Diagnostic Sciences and Special Therapies, University of Padova, Padova, Italy; and* [3]*Department of Anatomy and Cell Biology, McGill University, Montreal, Quebec, Canada*

Submitted 8 April 2014; accepted in final form 1 December 2014

Padda RS, Gkouvatsos K, Guido M, Mui J, Vali H, Pantopoulos K. A high-fat diet modulates iron metabolism but does not promote liver fibrosis in hemochromatotic Hjv$^{-/-}$ mice. *Am J Physiol Gastrointest Liver Physiol* 308: G251–G261, 2015. First published December 11, 2014; doi:10.1152/ajpgi.00137.2014.—Hemojuvelin (Hjv) is a membrane protein that controls body iron metabolism by enhancing signaling to hepcidin. Hjv mutations cause juvenile hemochromatosis, a disease of systemic iron overload. Excessive iron accumulation in the liver progressively leads to inflammation and disease, such as fibrosis, cirrhosis, or hepatocellular cancer. Fatty liver (steatosis) may also progress to inflammation (steatohepatitis) and liver disease, and iron is considered as pathogenic cofactor. The aim of this study was to investigate the pathological implications of parenchymal iron overload due to Hjv ablation in the fatty liver. Wild-type (WT) and Hjv$^{-/-}$ mice on C57BL/6 background were fed a standard chow, a high-fat diet (HFD), or a HFD supplemented with 2% carbonyl iron (HFD+Fe) for 12 wk. The animals were analyzed for iron and lipid metabolism. As expected, all Hjv$^{-/-}$ mice manifested higher serum and hepatic iron and diminished hepcidin levels compared with WT controls. The HFD reduced iron indexes and promoted liver steatosis in both WT and Hjv$^{-/-}$ mice. Notably, steatosis was attenuated in Hjv$^{-/-}$ mice on the HFD+Fe regimen. Hjv$^{-/-}$ animals gained less body weight and exhibited reduced serum glucose and cholesterol levels. Histological and ultrastructural analysis revealed absence of iron-induced inflammation or liver fibrosis despite early signs of liver injury (expression of α-smooth muscle actin). We conclude that parenchymal hepatic iron overload does not suffice to trigger progression of liver steatosis to steatohepatitis or fibrosis in C57BL/6 mice.

iron overload; hemochromatosis; nonalcoholic fatty liver disease; nonalcoholic steatohepatitis

BODY IRON HOMEOSTASIS IS CRUCIAL for health. Its misregulation may lead to iron deficiency or overload (10, 34). Hereditary hemochromatosis (HH) is one of the most frequent inherited disorders in Caucasians and is characterized by systemic iron overload (29). HH is etiologically linked to blunted expression of hepcidin, a liver-derived iron regulatory peptide hormone. Hepcidin insufficiency is typically caused by pathogenic mutations in the upstream regulator high iron (HFE) or other regulatory proteins such as transferrin receptor (TfR) 2 or hemojuvelin (HJV) (13). This causes hyperabsorption of dietary iron by intestinal enterocytes and uncontrolled release of iron from tissue macrophages to the plasma. As a result, transferrin saturation gradually increases and excessive non-transferrin bound iron accumulates, which is eventually taken up by hepatocytes and other tissue parenchymal cells. The most frequent form of HH is associated with HFE inactivation due to C282Y or, to a lesser extent, H63D or S65C point mutations (29). The clinical penetrance of HH may substantially differ among individuals with the same HFE genotype and is affected by gender, race, as well as genetic and environmental factors (2). Phenotypic variations are also evident in mouse models of HH, where Hfe$^{-/-}$ mice on different genetic backgrounds manifest variable degrees of iron overload (9).

Iron is potentially toxic due to its redox reactivity, which catalyzes the propagation of hydroxyl radicals by Fenton chemistry (12). Hepatic iron overload leads to oxidative stress and poses a risk factor for chronic liver disease, such as fibrosis, cirrhosis, and hepatocellular cancer (HCC) (31). On the other hand, other causes of liver injury, such as chronic hepatitis C, alcoholic liver disease, nonalcoholic fatty liver disease (NAFLD), or nonalcoholic steatohepatitis (NASH) are often associated with mild to moderate increase in hepatic iron levels, which is thought to aggravate liver damage (34). Non-hemochromatotic patients with NASH and parenchymal hepatic iron accumulation (39) or homo/heterozygocity for HFE mutations (14, 23) were identified to have increased risk for liver fibrosis. Similar results were reported for hemochromatotic patients with HFE C282Y mutations and NAFLD (30). Along these lines, Hfe$^{-/-}$ mice fed with a high-fat diet developed a NASH-like phenotype and early fibrosis, whereas wild-type (WT) control animals merely manifested hepatic steatosis in the absence of inflammation or liver injury (38). These findings indicate synergies between iron and lipid metabolism and fibrogenetic pathways. The underlying mechanisms remain elusive, but it is perceived that the predisposition of an HFE-deficient fatty liver to fibrosis is linked to iron overload (4, 24).

To explore the role of iron as a profibrogenic factor in the context of fatty liver, we used Hjv$^{-/-}$ mice, a model of juvenile hemochromatosis (JH). This disease is a rare variant of HH that is caused by functional inactivation of HJV (28), a bone morphogenetic protein (BMP) coreceptor that enhances iron-dependent signaling to hepcidin via the BMP/mothers against decapentaplegic pathway (1). JH is characterized by early onset and leads to cardiac, hepatic, and endocrine complications. Hjv$^{-/-}$ mice recapitulate the iron overload phenotype of JH patients but do not develop spontaneous liver fibrosis (17). This holds true for most mouse models of hemochromatosis, indicating that mice are somehow protected from iron-induced liver injury (9). Nevertheless, Hjv$^{-/-}$ mice ex-

Address for reprint requests and other correspondence: K. Pantopoulos, Lady Davis Institute for Medical Research, Jewish General Hospital, 3755 Cote-Ste-Catherine Rd., Montreal, Quebec, Canada H3T 1E2 (e-mail: kostas.pantopoulos@mcgill.ca).

hibit early signs of latent liver fibrogenesis and develop accelerated liver fibrosis in response to carbon tetrachloride (CCl_4) treatment (33). These experimental findings suggest that hepatic iron overload requires additional pathogenic stimuli (such as CCl_4) to induce liver fibrogenesis. Here, we examined whether hepatic steatosis suffices to trigger liver fibrogenesis in hemochromatotic $Hjv^{-/-}$ mice.

MATERIALS AND METHODS

Animals. Ten-week-old WT and $Hjv^{-/-}$ mice on C57BL/6 background (15) were placed on a normal diet (ND), a high-fat diet (HFD; Harlad Teklad TD.88137), or a HFD supplemented with 2% carbonyl iron (HFD+Fe) for 12 wk. The iron content of the HFD was similar to that of the ND. Each dietary group consisted of five to six male animals. The diet composition is shown in Tables 1 and 2. The mice were housed in a temperature-controlled environment (22 ± 1°C, 60 ± 5% humidity), with a 12:12-h light-dark cycle and were allowed ad libitum access to diets and drinking water. At the endpoint, the animals were killed under general anesthesia. Serum was obtained by cardiac puncture and stored at −80°C. Livers were rapidly excised, and tissue sections were either snap-frozen in liquid nitrogen or fixed in 10% neutral-buffered formalin, and then embedded in paraffin for histological and ultrastructural analysis. All animal procedures were approved by the Animal Care Committee of McGill University (protocol 4966).

Serum biochemistry. Transferrin saturation and serum iron, glucose, cholesterol, triglycerides, and transaminases [alanine aminotransferase (ALT), aspartate aminotransferase (AST)] were measured with a Roche Hitachi 917 Chemistry Analyzer at the Biochemistry Department of the Jewish General Hospital.

Quantification of nonheme iron. Hepatic nonheme iron was measured by the ferrozine assay (5). Results are expressed as micrograms of iron per gram of dry tissue weight.

Histological analysis. Tissue specimens were fixed in 10% buffered formalin and embedded in paraffin. To visualize ferric iron deposits, deparaffinized tissue sections were stained with Perls' Prussian blue. To ascertain the presence of steatosis and inflammation, hematoxylin and eosin (H&E) staining was performed, and slides were graded by an experienced pathologist according to standard criteria (33). Fibrosis was assessed following Sirius red staining.

Ultrastructural analysis. Liver tissues were dissected in 1 mm^3 for morphological studies by transmission electron microscopy (TEM). After two washes with ice-cold 0.2 M sodium cacodylate buffer containing 0.1% calcium chloride, pH 7.4, samples were fixed overnight at 4°C in 2.5% glutaraldehyde and washed three times with washing buffer. Pellets were postfixed with 1% aqueous OsO_4 + 1.5% aqueous potassium ferrocyanide for 1 h and washed three times with washing buffer. Specimens were dehydrated in a graded alcohol series, infiltrated with graded epon-alcohol and embedded in epon. Sections were polymerized at 58°C for 48 h. Ultrathin sections (90–100 nm thick) were prepared with a diamond knife using a Reichert Ultracut E-ultramicrotome, placed on 200-mesh copper grids, and stained with 2% uranyl acetate for 6 min and Reynold's lead for 5 min. TEM grids were examined with a Tecnai 12 120 kV TEM equipped with a Gatan 792 Bioscan CCD Camera (Gatan, Pleasanton, CA).

Quantitative real-time PCR. Total RNA was isolated from frozen liver tissues using the RNeasy Mini kit (Qiagen), and quality was assessed by determining the 260- to 280-nm absorbance ratios and by agarose gel electrophoresis. Quantitative real-time PCR was performed by using gene-specific primers (Table 3), with ribosomal protein 18S as the housekeeping gene for normalization (33). Data are reported as fold increases compared with samples from WT mice on normal diet ("control").

Western blotting. Liver extracts were prepared as previously described (33), and samples containing 30 μg of protein were analyzed by SDS-PAGE on a 10% gel. Following transfer of the proteins onto nitrocellulose filters (Bio-Rad), the blots were saturated with 5% nonfat milk in Tris-buffered saline (TBS) containing 0.1% (vol/vol) Tween 20 (TBS-T) and probed with 1:1,000 diluted ferritin (Novus), TfR1 (Zymed), or α-smooth muscle actin (α-SMA; Sigma) antibodies. After three washes with TBS-T, the blots were incubated with 1:5,000 diluted peroxidase-coupled goat anti-rabbit IgG (Sigma). The peroxidase signal was detected by enhanced chemiluminescence with the Western Lightning ECL kit (Perkin Elmer).

Statistical analysis. Quantitative data are expressed as means ± SD. Statistical analysis across multiple groups was performed by one-way ANOVA with Dunnett's test comparing each experimental group with the control (WT mice on ND). Two-way ANOVA with Bonferroni posttest comparison with the control was used for analyzing kinetics in multiple groups. For dietary treatments, comparisons were made within each genotype by two-tailed Student's *t*-test. The GraphPad Prism software (version 5.0d) was used for all statistical analyses. A probability value $P < 0.05$ was considered statistically significant.

Table 1. *Dietary composition of experimental diets*

	Normal Diet (Standard Chow)		High-Fat Diet	
Macronutrients	% by weight	%kcal from	% by weight	%kcal from
Protein	19		17.8	15.2
Carbohydrate	44		48.5	42.7
Fat	9	22	21.2	42.0
Total calories, kcal/g	3.30		4.5	

Table 2. *Ingredients used in experimental diets*

Ingredients	g/kg
Casein	195.0
DL-Methionine	3.0
Sucrose	341.46
Corn Starch	150.0
Anhydrous Milk Fat	210.0
Cholesterol	1.5
Cellulose	50.0
Mineral Mix	35.0
Calcium Carbonate	4.0
Vitamin Mix	10.0
Ethoxyquin, antioxidant	0.04

RESULTS

Effects of diets and genotypes on body weight. The body weight of all animals was monitored at various time intervals throughout the 12-wk experimental period. As expected, mice on HFD exhibited significantly increased body weight ($P < 0.001$) compared with isogenic controls on ND (Fig. 1*A*). $Hjv^{-/-}$ mice tended to gain less weight over time compared with WT controls, in both ND and HFD groups. After 8 wk, the weights of WT mice on ND and $Hjv^{-/-}$ mice on HFD were similar. Notably, the presence of 2% carbonyl iron within the HFD+Fe regimen completely prevented HFD-associated weight gain in all animals ($P < 0.001$), independent of genotype. This was not linked to any apparent reduction in food consumption and may be related to adipose tissue dystrophy that has been reported in WT mice fed with an iron-enriched diet (8). A representative image of WT mice after 12 wk of feeding with HFD or HFD+Fe is shown in Fig. 1*B*.

Table 3. *List of primers used for qPCR*

Gene	Accession No.	Forward Primer	Reverse Primer
r18S	NR_003278	GAATAATGGAATAGGACCGCGG	GGAACTACGACGGTATCTGATC
Hamp1 (hepcidin)	NM_032541	AAGCAGGGCAGACATTGCGAT	CAGGAT GTGGCTCTAGGCTATGT
AdipoR2	NM_197985	GGCAGATAGGCTGGCTAATGC	GGAAGAGCTGATGAGAGTGAAACC
Ppar-α	NM_011144.6	CATGTGAAGGCTGTAAGGGCTT	TCTTGCAGCTCCGATCACACT
Hmgcr	NM_008255.2	CATGGTTCACAACAGATCAAAGATAAAT	TGCCTTCTTGGTGCACGTT
Tnf-α	NM_013693.3	CCAGACCCTCACACTCAGATCA	CACTTGGTGGTTTGCTACGAC
α_1-(I)-collagen	NM_007742	CCAAGGGTAACAGCGGTGAA	CCTCGTTTTCCTTCTTCTCCG
Et-1	NM_010104	GAAACAGCTGTCTTGGGAGC	AGTTCTTTTCCTGCTTGGCA
Pdgf	NM_027924	ACTCTCACTGCTGATGCCCT	GACTGCATTGGTCAGCTTCA

r18S, ribosomal protein 18S; AdipoR2, adiponectin receptor 2; Ppar-α, peroxisome proliferator-activated receptor-α; Hmgcr, 3-hydroxy-3-methylglutarate-coenzyme A reductase; Tnf-α, tumor necrosis factor-α; Et-1, endothelin-1; Pdgf, platelet-derived growth factor.

Effects of diets and genotypes on iron metabolism. Hjv$^{-/-}$ mice provide an established model of systemic iron overload (15, 17). This is reflected in hyperferremia (serum iron: 42.6 ± 1.1 vs. 22.2 ± 0.9 μmol/l in WT, $P < 0.001$), high Tf saturation (87 vs. 40% in WT, $P < 0.001$), pathological hepatic iron content (6,273 ± 602 vs. 433 ± 52 μg iron/g of dry liver in WT, $P < 0.001$), and histologically detectable iron deposits in the liver parenchyma (Fig. 2). Feeding with the HFD significantly decreased serum iron concentration (from 42.6 ± 1.1 to 35 ± 5.4 μmol/l, $P < 0.05$), Tf saturation (from 87 to 67%, $P < 0.001$), and hepatic iron content (from 6,273 ± 602 to 3,858 ± 271 μg iron/g of dry liver, $P < 0.01$) in Hjv$^{-/-}$ mice. Likewise, the HFD significantly decreased Tf saturation (from 40 to 35%, $P < 0.05$) and hepatic iron content (from 433 ± 52 to 243 ± 50 μg iron/g of dry liver, $P < 0.01$) in WT mice. The HFD+Fe regimen boosted serum and hepatic iron in both WT and Hjv$^{-/-}$ mice to levels that were indistinguishable between the two genotypes. These data suggest that HFD intake modulates iron metabolism and reduces iron indexes in WT and Hjv$^{-/-}$ mice.

As expected, the expression of hepcidin mRNA was miniscule in Hjv$^{-/-}$ mice (Fig. 3*A*). HFD intake decreased hepcidin mRNA levels by 60% ($P < 0.05$) in WT mice, but no statistically significant difference was observed in Hjv$^{-/-}$ mice. WT mice on combined HFD+Fe exhibited 7.3-fold higher hepcidin mRNA levels vs. WT mice on ND ($P < 0.001$). Likewise, hepcidin mRNA expression was increased 3.8-fold ($P < 0.05$) in Hjv$^{-/-}$ mice on HFD+Fe vs. ND.

The expression of TfR1, a protein involved in cellular iron uptake (40), was evident in livers of WT mice on ND, whereas expression of the iron storage protein ferritin was undetectable (Fig. 3*B*). Conversely, Hjv$^{-/-}$ mice on ND exhibited a low TfR1 content and expressed high levels of ferritin, consistent with their high iron load. The HFD augmented TfR1 expression in both genotypes without affecting ferritin levels, in line with the HFD-related reduction of hepatic iron content. The combined HFD+Fe regimen diminished TfR1 and induced ferritin expression in WT livers. Densitometric quantification of the Western blotting data is provided in Fig. 3, *C* and *D*.

Effects of diets and genotypes on glucose and lipid metabolism. Hjv$^{-/-}$ mice manifested a 25% decrease ($P < 0.001$) in serum glucose levels vs. WT animals (Fig. 4*A*). This finding corroborates similar observations in isogenic Hfe$^{-/-}$ mice and could be explained by enhanced insulin sensitivity due to local adipocyte iron deficiency, followed by glucose clearance in skeletal muscles (11, 18). Serum glucose values of WT mice were increased by 8% ($P < 0.05$) in response to HFD intake. A similar trend was evident in Hjv$^{-/-}$ mice; however, no statistical significance was reached. The presence of dietary carbonyl iron completely abolished HFD-related hyperglycemia and, moreover, led to a significant 25% ($P < 0.001$) reduction of serum glucose concentrations in both genotypes; the reason for this is obscure. As expected, the HFD promoted a twofold ($P < 0.001$) increase of serum cholesterol levels in both WT and Hjv$^{-/-}$ mice (Fig. 4*B*). Administration of HFD+Fe restored physiological serum cholesterol values in WT mice but did not prevent hypercholesterolemia in Hjv$^{-/-}$ animals. Serum triglyceride levels (Fig. 4*C*) were significantly increased by HFD intake in WT mice (30%, $P < 0.01$) and by the HFD+Fe regimen in both WT (1.5-fold, $P < 0.001$) and Hjv$^{-/-}$ (1.3-fold, $P < 0.01$) mice, possibly as a result of increased release of fatty acids from visceral adipose tissue. All WT and Hjv$^{-/-}$ mice of the HFD group developed severe hepatic steatosis (with >30% of hepatocytes affected). The type of steatosis was either macrovesicular or microvesicular

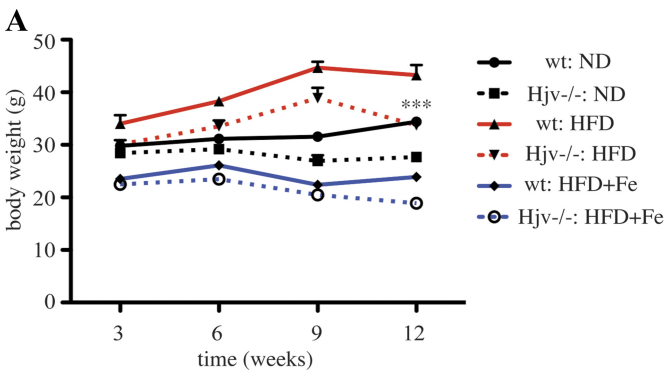

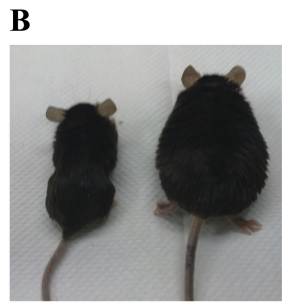

Fig. 1. Growth of wild-type (WT) and hemojuvelin-deficient (Hjv$^{-/-}$) mice depends on diet and genotype. Ten-week-old WT and Hjv$^{-/-}$ mice (n = 5 or 6 males/group) were placed on a normal diet (ND), a high-fat diet (HFD), or a HFD supplemented with 2% carbonyl iron (HFD+Fe) for 12 wk, and weight gain was monitored every 3 wk. *A*: mouse body weights are plotted against time. The genotypes and the dietary regimens are indicated on the *right*. *B*: representative image of WT mice on HFD without (*left*) or with (*right*) carbonyl iron supplementation. ***$P < 0.001$ (2-way ANOVA vs. control).

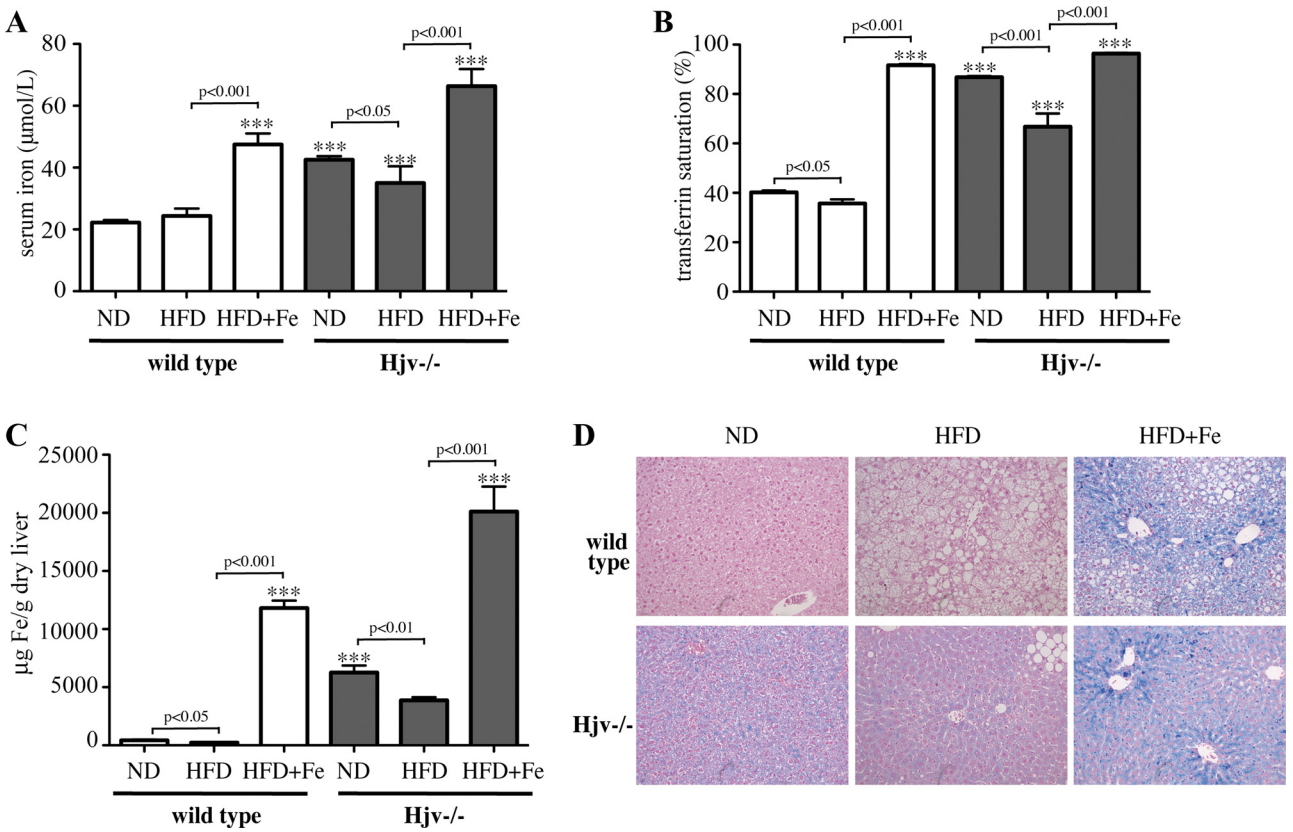

Fig. 2. HFD intake reduces iron indexes in WT and Hjv$^{-/-}$ mice. At the endpoint, the mice described in Fig. 1 were exsanguinated and killed, and blood and tissues were analyzed as described in Figs. 2–9. *A*: analysis of serum iron. *B*: analysis of transferrin saturation. *C*: quantification of hepatic nonheme iron content by the ferrozine assay. *D*: histological detection of iron deposits in liver sections by Perls' iron staining. Original magnification: ×20. ***$P < 0.001$ (1-way ANOVA vs. control); comparisons within each genotype were performed by 2-tailed Student's *t*-test.

and did not correlate with the genotype of the mice. The degree of steatosis was substantially reduced in Hjv$^{-/-}$ mice fed HFD+Fe (Fig. 4*D*, see also Fig. 6*C*).

Adiponectin is an insulin-sensitizing protein hormone that modulates a number of metabolic processes, including glucose metabolism and fatty acid oxidation (7). It is secreted by adipose tissues and acts via the two major receptors, AdipoR1 and AdipoR2, which are expressed in the muscles and liver, respectively. AdipoR2 inhibits lipogenesis and activates peroxisome proliferator-activated receptor (Ppar)-α and fatty acid oxidation genes. Hepatic AdipoR2 mRNA was induced by HFD in both WT and Hjv$^{-/-}$ mice, but this effect was antagonized by the HFD+Fe regimen (Fig. 5*A*). Similar responses were observed in the expression of Ppar-α mRNA (Fig. 5*B*). We also analyzed expression of the mRNA encoding 3-hydroxy-3-methylglutarate-coenzyme A reductase (Hmgcr), an enzyme catalyzing the rate-limiting step for cholesterol biosynthesis that was found to be positively regulated by hepatic iron (16). Surprisingly, hepatic Hmgcr mRNA levels were not increased in Hjv$^{-/-}$ mice, whereas HFD negatively regulated its expression (Fig. 5*C*). The HFD+Fe regimen promoted a robust 3.3-fold induction ($P < 0.001$) of Hmgcr mRNA in WT mice, consistent with iron regulation (16), but not in Hjv$^{-/-}$ mice. Together, the data in Figs. 4 and 5 suggest that HFD intake affects lipid metabolism in both WT and Hjv$^{-/-}$ mice.

Parenchymal iron overload does not suffice to promote progression of hepatic steatosis to steatohepatitis or fibrosis in Hjv$^{-/-}$ and WT mice. Hjv$^{-/-}$ mice exhibited elevated values of liver-derived serum transaminases compared with WT controls (ALT: 68.8 ± 7.3 vs. 24.6 ± 1.5 IU/l in WT, $P < 0.001$; and AST: 145.7 ± 13.5 vs. 55.2 ± 6.0 IU/l in WT, $P < 0.001$), which is indicative of liver injury (Fig. 6, *A* and *B*). Surprisingly, these values were not further augmented by HFD intake but were rather significantly decreased (ALT: from 68.8 ± 7.3 to 34.6 ± 5.7 IU/l, $P < 0.001$; and AST: from 145.7 ± 13.5 to 74.2 ± 8.8 IU/l, $P < 0.001$). By contrast, the HFD increased liver transaminases in WT mice (ALT: from 24.6 ± 1.4 to 88.4 ± 23.0 IU/l, $P < 0.001$; and AST: from 55.2 ± 6.0 to 100.1 ± 15.1 IU/l, $P < 0.001$). Combined HFD+Fe administration reversed the effects of HFD on transaminases in WT mice and on AST in Hjv$^{-/-}$ mice. The reason for this unexpected finding is not known.

Histological analysis of liver sections by H&E staining did not show any signs of iron-induced necroinflammation or fibrosis in Hjv$^{-/-}$ or WT mice (Fig. 6*C*). Areas with limited infiltration of inflammatory cells were only documented in the liver of one WT mouse on HFD and another WT mouse on HFD+Fe (data not shown). The absence of fibrosis in any of the mouse livers was confirmed by the lack of detectable collagen fibers after staining with Sirius red (data not shown). Biochemical analysis uncovered a tendency for increased ex-

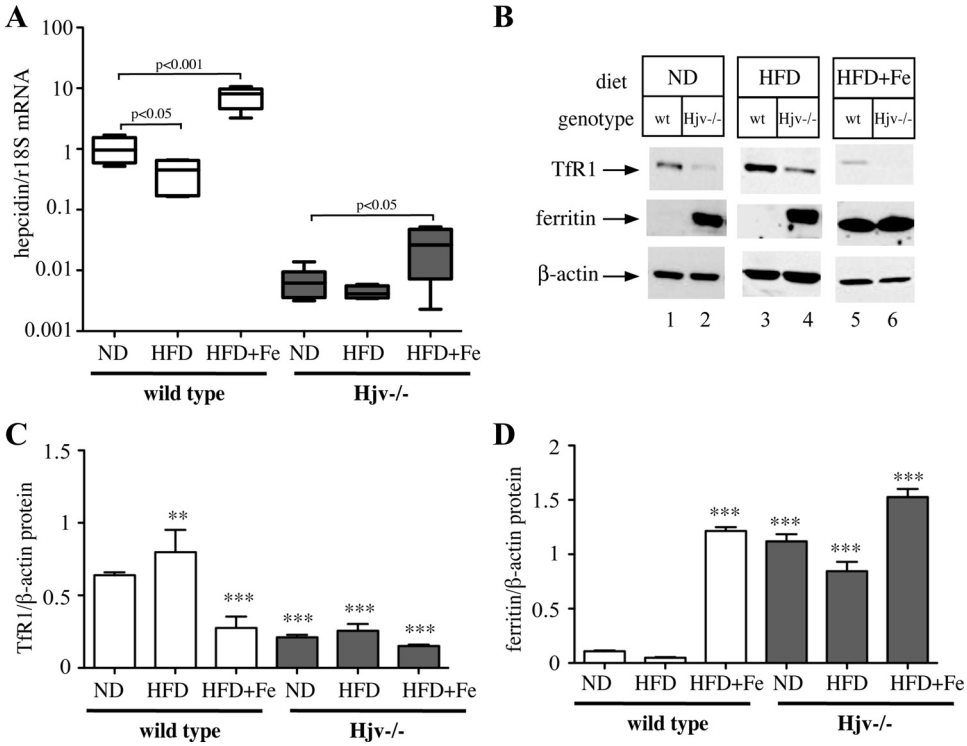

Fig. 3. HFD intake leads to relative iron deficiency in hepatocytes. *A*: analysis of hepatic hepcidin mRNA expression by quantitative real-time PCR (qPCR). Comparisons within each genotype were performed by 2-tailed Student's *t*-test. *B*: analysis of hepatic expression of transferrin receptor (TfR) 1, ferritin, and control β-actin by Western blotting. *C* and *D*: densitometric quantification of the Western blot data shown in *B*. The *y*-axes indicate relative expression of TfR1 (*A*) or ferritin (*B*) normalized to β-actin. Data correspond to 3 experiments. $^{**}P < 0.01$ and $^{***}P < 0.001$ (1-way ANOVA vs. control).

pression of the mRNAs encoding the inflammatory marker tumor necrosis factor-α and the fibrosis markers α_1-(I)-collagen, endothelin-1, and platelet-derived growth factor in livers of both WT and Hjv$^{-/-}$ on HFD (Fig. 7). However, there were no significant differences among the genotypes, and the values tended to normalize following HFD+Fe intake.

Ultrastructural analysis of liver sections with TEM further validated the absence of necroinflammation or fibrosis (Fig. 8). Livers of WT mice on ND contained regular lipid droplets and glycogen granules (Fig. 8*A*). The density of glycogen clusters was drastically reduced in livers of Hjv$^{-/-}$ mice on ND, whereas there was an increase in distribution of well-organized endoplasmic reticulum (see high magnification). There was no evidence for presence of lipid droplets in these samples. Following HFD intake, the lipid droplet content was dramatically increased in WT and modestly increased in Hjv$^{-/-}$ mouse livers (Fig. 8*B*). Lipid droplets of WT mice exhibited dark spots, which may represent ferritin. The presence of

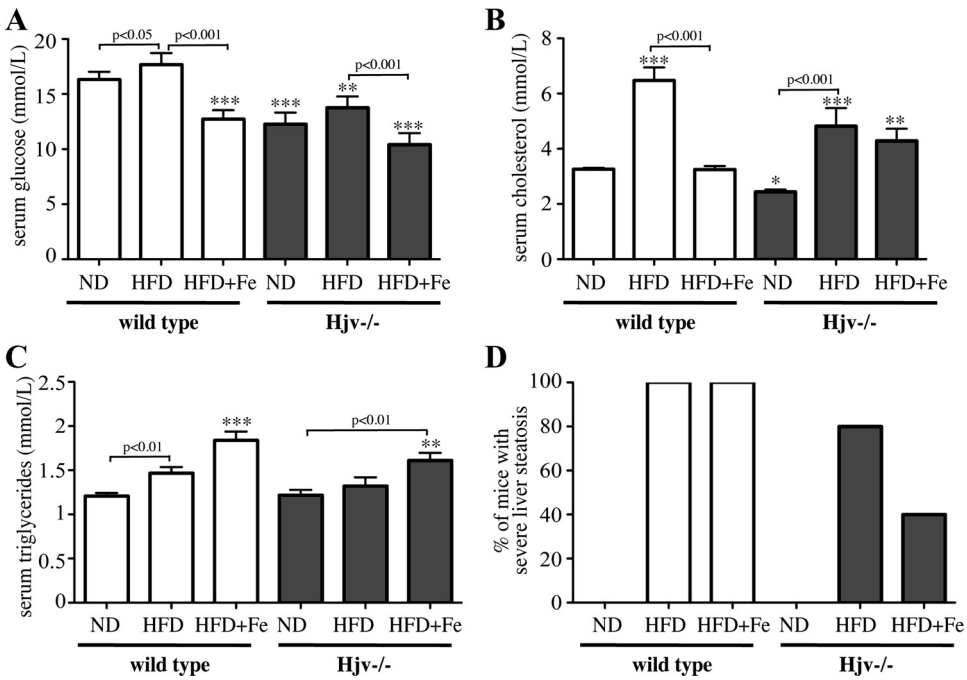

Fig. 4. HFD intake increases serum glucose and cholesterol levels and leads to fatty liver. *A*: analysis of serum glucose. *B*: analysis of serum cholesterol. *C*: analysis of serum triglycerides. *D*: semiquantitative grading of liver steatosis; data are compiled from all mice. $^{*}P < 0.05$, $^{**}P < 0.01$, and $^{***}P < 0.001$ (1-way ANOVA vs. control); comparisons within each genotype were performed by 2-tailed Student's *t*-test.

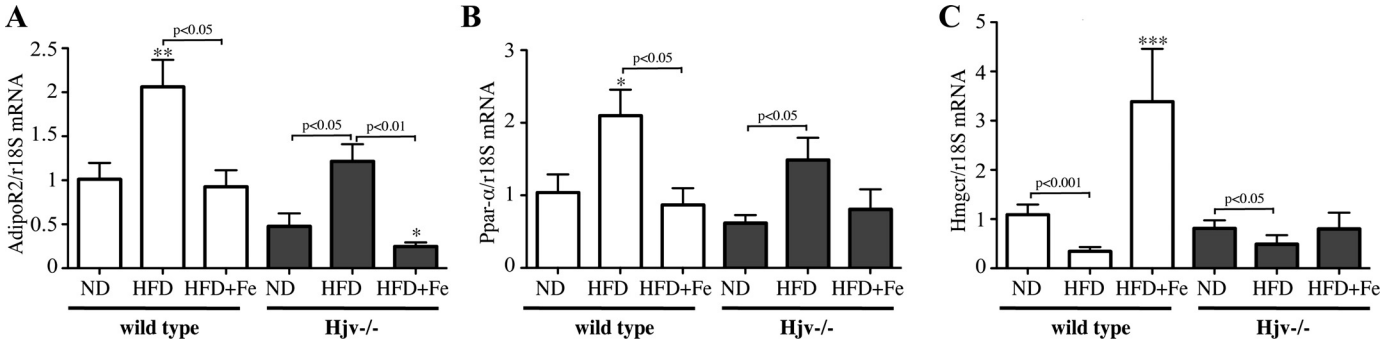

Fig. 5. HFD intake modulates hepatic lipid metabolism. The expression of adiponectin receptor (AdipoR) 2 mRNA (*A*), peroxisome proliferator-activated receptor (PPAR)-α mRNA (*B*), and 3-hydroxy-3-methylglutarate-coenzyme A reductase (Hmgcr) mRNA (*C*) were analyzed from mouse livers by qPCR. $*P < 0.05$, $**P < 0.01$, and $***P < 0.001$ (1-way ANOVA vs. control); comparisons within each genotype were performed by 2-tailed Student's *t*-test.

carbonyl iron in the HFD+Fe diet reduced lipid content in both WT and Hjv$^{-/-}$ mouse livers (Fig. 8*C*). In these samples, we observed accumulation of membrane-bound vesicles (lysosomes, microphagosomes) containing high-contrast ferritin-like nanoparticles. The overall architecture of mitochondria did not appear to be affected by the genotype or diet.

Western blot analysis detected low expression of α-SMA in livers of ~50% of Hjv$^{-/-}$ mice on ND, whereas the remaining animals were negative. Representative images are shown in Fig. 9*A* (*lanes 3* and *4*), and densitometric quantification is provided in Fig. 9*B*. This result contrasts the strong expression of α-SMA in livers of naïve Hjv$^{-/-}$ mice on mixed 129S6/SvEvTac genetic background, which was reported previously (33). Parallel analysis of liver samples from naïve Hjv$^{-/-}$ mice in mixed 129S6/SvEvTac or pure C57BL/6 (B6) backgrounds reproduces the previous findings (Fig. 9*C*), suggesting that expression of this fibrosis marker depends on the Hjv$^{-/-}$ mouse strain. The HFD induced robust expression of α-SMA in C57BL/6 Hjv$^{-/-}$ mice and weaker expression in isogenic WT controls (Fig. 9*A*, compare *lanes 1–4* with *lanes 5–8*; see also Fig. 9*B*). Similar results were obtained with the HFD+Fe regimen, although the induction of α-SMA in C57BL/6 Hjv$^{-/-}$ mice was less pronounced compared with HFD alone (Fig. 9*A*, *lanes 9–12*; see also Fig. 9*B*). Thus, whereas both iron overload and HFD appear to promote latent hepatic fibrogenesis, they fail to synergistically induce histologically detectable liver fibrosis in Hjv$^{-/-}$ mice.

DISCUSSION

We show here that hemochromatotic Hjv$^{-/-}$ mice develop hepatic steatosis in response to HFD intake, which does not

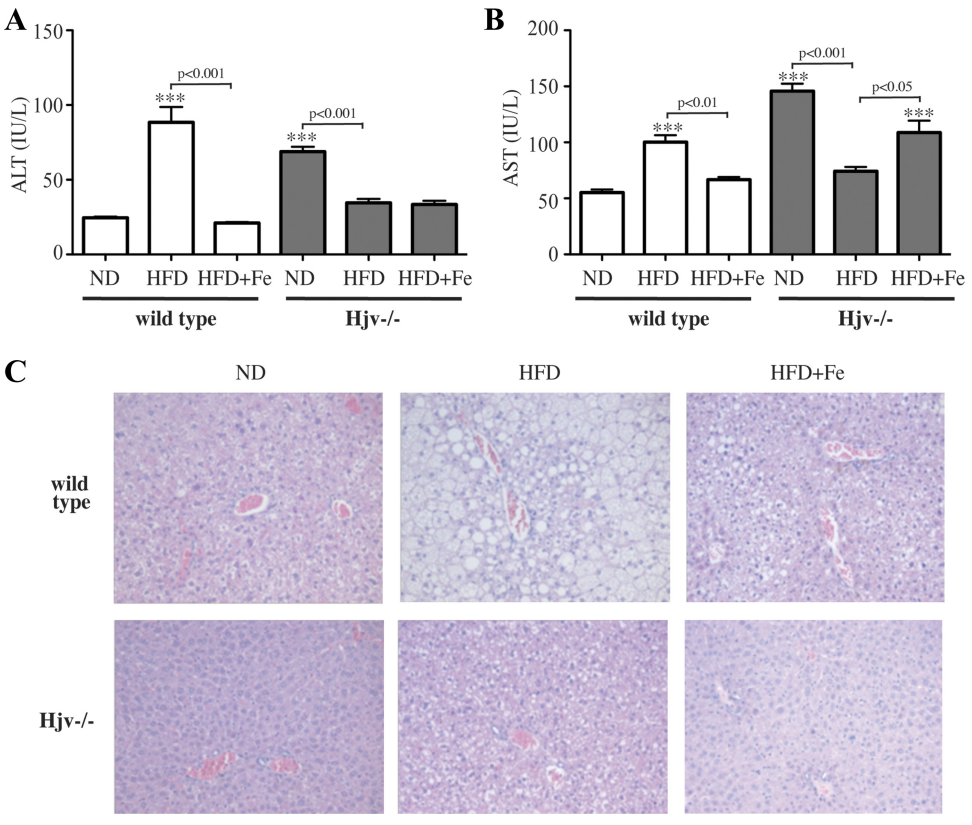

Fig. 6. Analysis of WT and Hjv$^{-/-}$ mice for serum transaminases and liver pathology. *A*: analysis of serum alanine aminotransferase (ALT). *B*: analysis of serum aspartate aminotransferase (AST). *C*: hematoxylin and eosin (H&E) staining in liver sections for assessment of tissue architecture, necroinflammation, and steatosis. Tissue architecture of WT and Hjv$^{-/-}$ livers was normal under all dietary regiments, and only steatosis but no necroinflammation was observed. Original magnification: ×20. $***P < 0.001$ (1-way ANOVA vs. control); comparisons within each genotype were performed by 2-tailed Student's *t*-test.

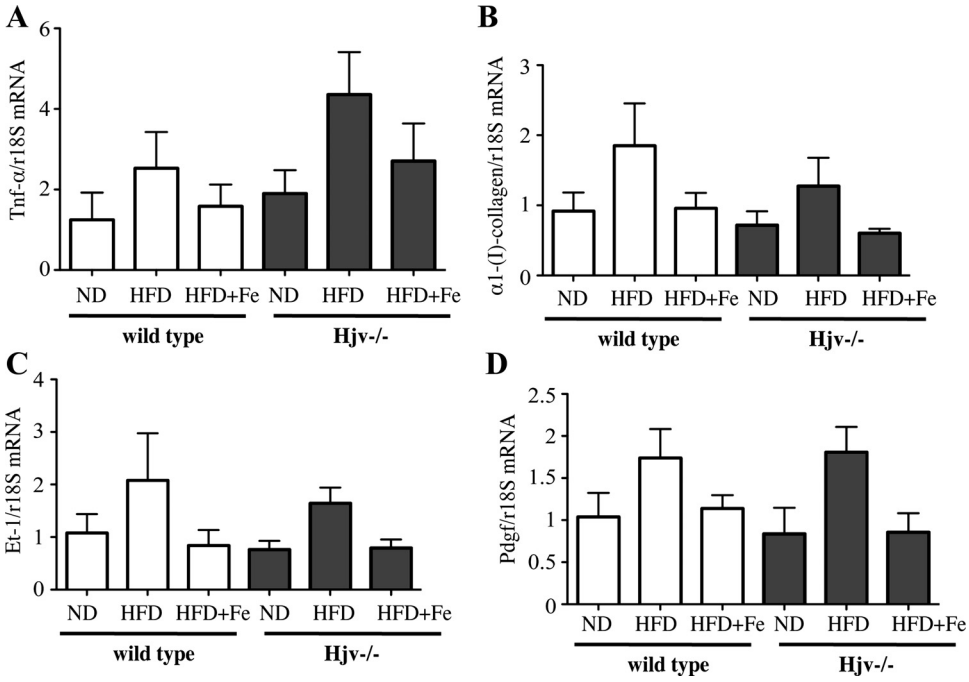

Fig. 7. qPCR analysis of liver cytokines in WT and Hjv$^{-/-}$ mice. *A*: expression of tumor necrosis factor-α (Tnf-α) mRNA. *B*: expression of α_1-(I)-collagen mRNA. *C*: expression of endothelin-1 (Et-1) mRNA. *D*: expression of platelet-derived growth factor (Pdgf) mRNA. Statistical analysis by 1-way ANOVA did not reveal significant differences in expression of each of these cytokines vs. control.

progress to an inflammatory or fibrotic stage, despite excessive parenchymal iron overload. Isogenic WT control mice with physiological hepatic iron content manifested similar pathology upon HFD feeding. Supplementation of the HFD with 2% carbonyl iron promoted hepatic iron overload in WT mice and further augmented the hepatic iron content of Hjv$^{-/-}$ mice, but likewise failed to trigger liver inflammation or fibrosis in both genotypes.

In humans with HH, hepatic steatosis is a known risk factor for development of liver fibrosis (30). Hepatic iron overload is considered as a pathogenic cofactor that can lead to progression of NAFLD to NASH and fibrosis (24). Nonhemochromatotic patients with NAFLD often present with mild hepatic iron overload, which predisposes to liver injury. Nevertheless, this appears to depend on the pattern of iron distribution among hepatocytes and Kupffer cells, which is not always consistent. Thus, liver biopsies from NAFLD patients may contain histologically stainable iron deposits in either hepatocytes, Kupffer cells, or both cell types (4, 24), underlying diverse etiologies for hepatic iron accumulation. A clinical study with a cohort of NAFLD patients from the United States reported association of iron overload in Kupffer cells with liver fibrosis (25). Reticuloendothelial iron overload was also found to correlate with progression of NASH to HCC in patients from Italy (37). Along these lines, experiments with a rabbit model of NASH suggested that iron loading of Kupffer cells via phagocytosis of apoptotic erythrocytes promotes liver fibrogenesis (26). However, another clinical study with patients from Italy concluded that progression of NAFLD to liver fibrosis correlates to parenchymal but not reticuloendothelial iron overload, independent of HFE mutations (39).

The Hjv$^{-/-}$ mouse model of HH is characterized by massive hepatic iron overload, where excess iron is exclusively distributed among hepatocytes, especially in periportal areas (17). We observed reduced density of glycogen granules and absence of lipid droplets in Hjv$^{-/-}$ livers, which indicates high metabolic activity and is consistent with the resistance of the Hjv$^{-/-}$ mice to HFD-induced obesity. The reason for these responses is unclear and deserves further investigation. Our overall data suggest that parenchymal iron overload is not a pathogenic cofactor for the development of liver injury in steatotic Hjv$^{-/-}$ mice. A previous study showed that Hfe$^{-/-}$ mice develop a NASH-like phenotype and early liver fibrosis in response to an 8-wk HFD feeding regimen (38). These animals represent another model of hemochromatosis with similar phenotypic features but milder degree of iron overload compared with Hjv$^{-/-}$ mice (38). The striking differences in the outcome of the HFD experiments reported herein and previously (38) cannot be attributed to spurious genetic background effects, since the Hfe$^{-/-}$ and Hjv$^{-/-}$ mice were backcrossed to the C57BL/6 strain. Moreover, the fat and carbohydrate composition, as well as the cholesterol content of the HFDs, did not differ substantially. It is tempting to speculate that the susceptibility of steatotic Hfe$^{-/-}$ mice to liver fibrosis is related to the lack of Hfe. This is an atypical major histocompatibility class I protein that operates upstream of the hepcidin pathway and is required for proper iron-dependent signaling (27). The exact function of HFE as regulator of hepcidin is not clear, and a role in antigen binding has been excluded for steric reasons. Nevertheless, HFE is capable of recognizing subsets of T lymphocytes and thereby has the potential of modulating immune responses (32). Along these lines, the development of HFD-induced steatosis in C57BL/6 mice has been associated with excessive production of proinflammatory cytokines by hepatic T lymphocytes (21). It is conceivable that the iron content of Hfe$^{-/-}$ mice may affect their susceptibility to develop HFD-induced liver fibrosis.

A characteristic feature of mouse models of HH (including Hjv$^{-/-}$ mice), which recapitulates human disease, is the iron-deficient phenotype of their macrophages, enterocytes, and adipocytes in spite of systemic iron overload (9, 11). This is caused by overexpression of ferroportin in these cell types due

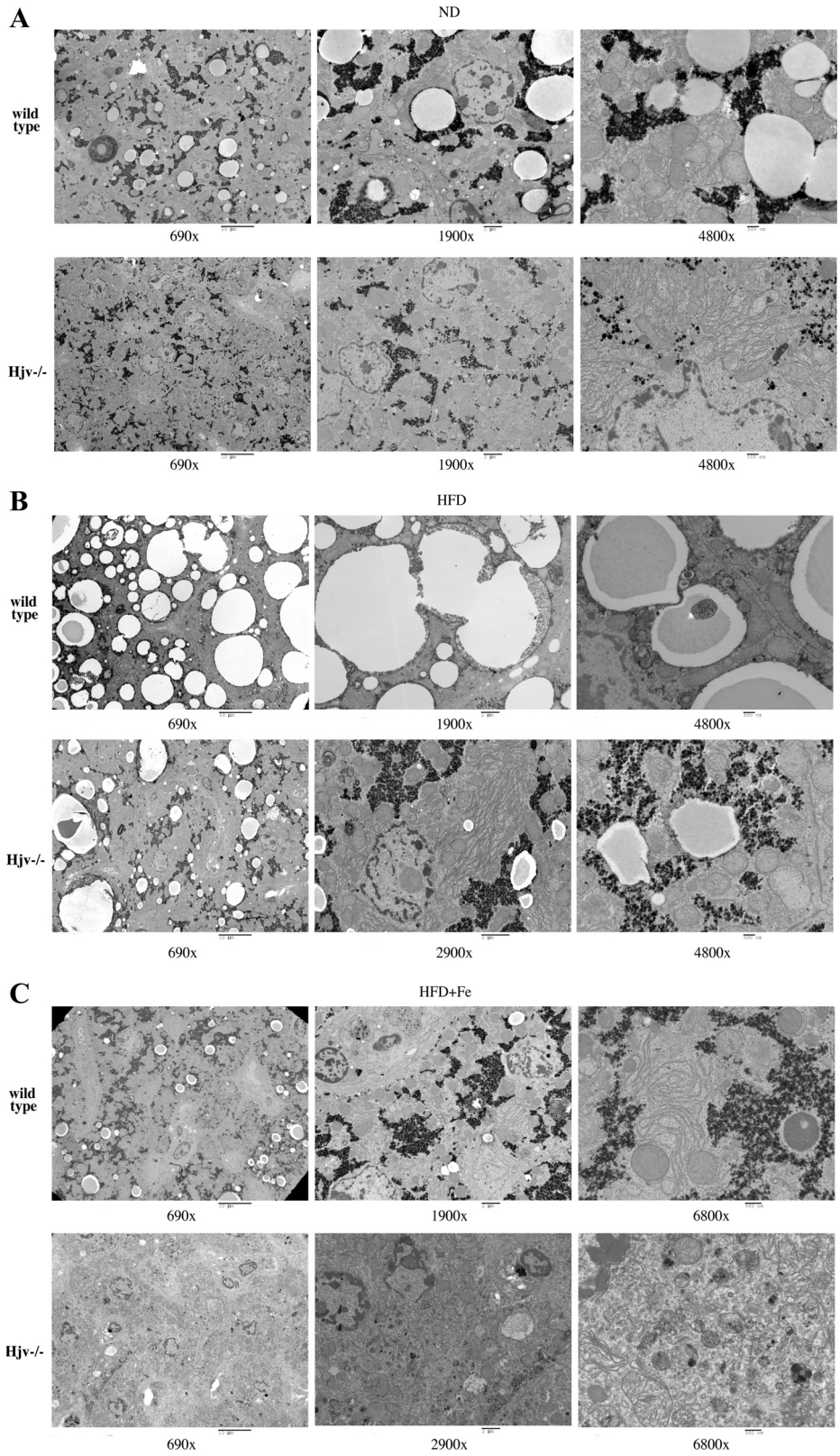

Fig. 8. Transmission electron microscopy (TEM) ultrastructural analysis of liver samples from WT and Hjv$^{-/-}$ mice following intake of ND (*A*), HFD (*B*), or HFD+Fe (*C*). Three magnifications are shown for each sample. The data demonstrate absence of necroinflammation or fibrosis and uncover morphological differences among genotypes and diets (see RESULTS).

to suppression of hepcidin. We recently showed that Hjv$^{-/-}$ mice on a high-iron diet (containing 2% carbonyl iron) induce residual hepcidin expression, which leads to partial, yet inappropriately low, retention of iron within splenic macrophages (15). The high-iron diet also increases splenic iron load in WT mice (5). Thus, it is plausible to assume that the HFD+Fe regimen promoted relative iron retention in Kupffer cells of Hjv$^{-/-}$ mice and iron loading in Kupffer cells of WT mice.

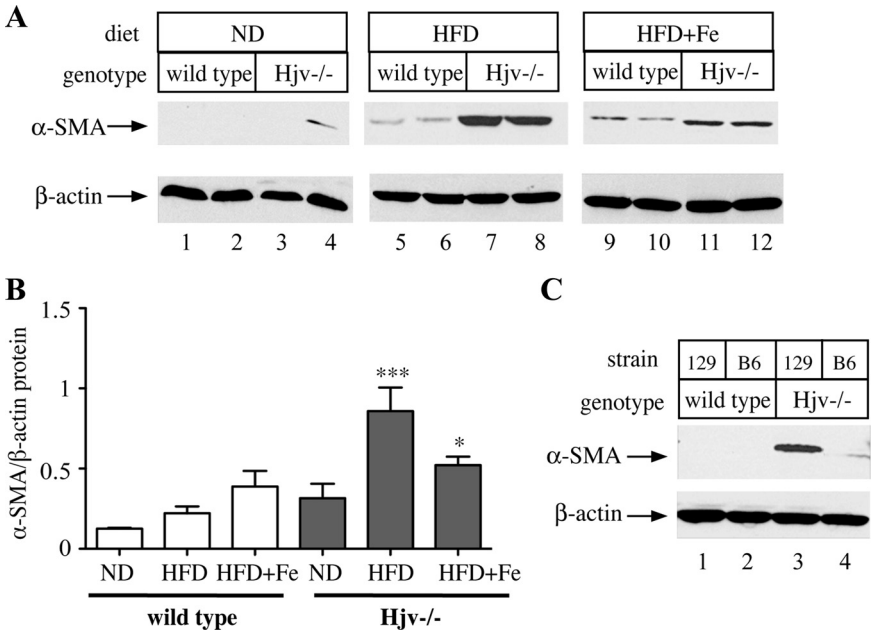

Fig. 9. Western blot analysis of smooth muscle actin (α-SMA) expression in livers of WT and Hjv$^{-/-}$ mice. *A*: control WT mice are negative for hepatic α-SMA, but ~50% of naïve Hjv$^{-/-}$ mice express low levels of this marker of liver fibrogenesis (*lanes 3–4*, representing one negative and one positive sample, respectively). HFD and HFD+Fe intake induces α-SMA expression in both WT and Hjv$^{-/-}$ mice. *B*: densitometric quantification of the Western blot data shown in Fig. 7*A*. The *y*-axis indicates relative expression of α-SMA normalized to β-actin. Data correspond to 3 experiments. *C*: the expression of α-SMA in livers of naïve Hjv$^{-/-}$ mice depends on the genetic background of the animals. Expression is robust in all 129S6/SvEvTac Hjv$^{-/-}$ mice (a representative example is shown in *lane 3*) and weak in the α-SMA-positive C57BL/6 (B6) Hjv$^{-/-}$ mice (*lane 4*). *$P < 0.05$ and ***$P < 0.001$ (1-way ANOVA vs. control).

Nevertheless, none of the two genotypes developed histologically or ultrastructurally detectable liver injury. It is possible that the amount of iron accumulated in Kupffer cells was below the threshold required to trigger liver fibrosis. Notably, neither Hjv$^{-/-}$ nor WT mice on HFD+Fe became obese (they failed to gain weight), whereas the Hjv$^{-/-}$ mice manifested a lower degree of hepatic steatosis. The latter did not have a healthy appearance during the last days of the dietary treatment and exhibited reduced activity in the cages. Therefore, the results with the HFD+Fe regimen should be interpreted with caution.

Another reason for the failure of genetic and/or dietary iron overload to catalyze the progression of steatosis to advanced liver injury might be related to the strain of the mice. Animals of the C57BL/6 genetic background are relatively resistant to CCl_4-induced liver fibrosis, and this is associated with altered T cell responses (35). Other strains are more sensitive, and hemochromatotic Hfe$^{-/-}$Tfr2$^{-/-}$ mice on the AKR background even develop spontaneous iron-induced liver fibrosis (6). The resistance of the C57BL/6 strain is also reflected in the weak α-SMA expression in livers of Hjv$^{-/-}$ mice backcrossed to pure C57BL/6 background compared with the profound α-SMA content in livers of Hjv$^{-/-}$ mice in mixed 129S6/SvEvTac background (Fig. 7*B*). The even low expression of hepatic α-SMA in naïve C57BL/6 Hjv$^{-/-}$ mice, as well as their increased serum ALT and AST values compared with that of WT controls, indicates that iron overload induces latent profibrogenic responses in these animals. However, an additional trigger is presumably required for the development of fibrosis. We previously showed that parenchymal iron overload promoted oxidative stress and accelerated CCl_4-induced liver fibrosis in 129S6/SvEvTac Hjv$^{-/-}$ mice (33). It will be interesting to examine the effects of HFD in this setting and, conversely, the effects of CCl_4 in C57BL/6 Hjv$^{-/-}$ mice. In addition, it will be important to address whether a longer period of HFD exposure could result in more significant liver injury.

Parenteral (19) or dietary (20) iron overload of Wistar or Fischer 344 rats, respectively, was shown to aggravate nutritional steatohepatitis caused by a methionine/choline-deficient diet. Although parenteral iron administration leads to both parenchymal and reticuloendothelial iron overload (5, 19), the adverse effects of dietary iron overload in the nutritional steatohepatitis rat model imply an increased sensitivity of rats to iron-induced hepatotoxicity compared with C57BL/6 mice. Feeding Sprague-Dawley rats with a HFD led to progressive hepatic iron accumulation and oxidative stress, which correlated with induction of iron regulatory protein 1 in hepatocytes, and concomitant modulation of its downstream targets TfR1 and ferritin (22). Increased hepatic iron uptake via TfR1 was associated with upregulation of hepcidin mRNA and inflammation. In agreement with these findings, the data in Fig. 3 show HFD-dependent stimulation of hepatic TfR1 in both WT and Hjv$^{-/-}$ mice. However, this did not correlate to any increases in serum or hepatic iron indexes, which were rather reduced (Fig. 2). Thus, the stimulation of hepatic TfR1 in mice fed the HFD, in the presence of reduced hepatic iron content, may represent a response to relative iron deficiency. This interpretation is also supported by the downregulation of hepcidin mRNA in HFD-fed WT mice (Fig. 3*A*). An analogous suppression of hepcidin, associated with decreased hepatic iron content, was observed upon feeding C57BL/6 mice with a HFD for 16 wk (3). Moreover, feeding C57BL/6 mice with a HFD has also been associated with hepcidin-independent iron deficiency due to reduced intestinal iron absorption (36).

In conclusion, our data demonstrate that parenchymal iron overload is not a pathogenic cofactor for progression of liver steatosis to steatohepatitis or fibrosis in Hjv$^{-/-}$ (and WT) mice of C57BL/6 background. The existence of iron- resistant and -sensitive mouse strains implies the involvement of further genetic factors in the development of iron-dependent liver fibrogenesis, which remain to be identified and characterized.

ACKNOWLEDGMENTS

We thank Drs. Naciba Benlimame and Alan Spatz for assistance with histology.

GRANTS

This work was supported by a grant from the Canadian Institutes for Health Research (MOP-86514). K. Pantopoulos was holder of a Chercheur National career award from the Fonds de la Recherche en Santé du Quebéc (FRSQ). K. Gkouvatsos was a recipient of an FRSQ doctoral fellowship.

DISCLOSURES

No conflicts of interest, financial or otherwise, are declared by the authors.

AUTHOR CONTRIBUTIONS

Author contributions: R.S.P., K.G., and J.M. performed experiments; R.S.P., M.G., and H.V. analyzed data; R.S.P., M.G., H.V., and K.P. interpreted results of experiments; R.S.P. and K.P. prepared figures; M.G., J.M., H.V., and K.P. approved final version of manuscript; K.P. conception and design of research; K.P. drafted manuscript; K.P. edited and revised manuscript.

REFERENCES

1. **Babitt JL, Huang FW, Wrighting DM, Xia Y, Sidis Y, Samad TA, Campagna JA, Chung RT, Schneyer AL, Woolf CJ, Andrews NC, Lin HY.** Bone morphogenetic protein signaling by hemojuvelin regulates hepcidin expression. *Nat Genet* 38: 531–539, 2006.
2. **Beutler E.** The HFE Cys282Tyr mutation as a necessary but not sufficient cause of clinical hereditary hemochromatosis. *Blood* 101: 3347–3350, 2003.
3. **Chung J, Kim MS, Han SN.** Diet-induced obesity leads to decreased hepatic iron storage in mice. *Nutr Res* 31: 915–921, 2011.
4. **Corradini E, Pietrangelo A.** Iron and steatohepatitis. *J Gastroenterol Hepatol* 27, *Suppl* 2: 42–46, 2012.
5. **Daba A, Gkouvatsos K, Sebastiani G, Pantopoulos K.** Differences in activation of mouse hepcidin by dietary iron and parenterally administered iron dextran: compartmentalization is critical for iron sensing. *J Mol Med (Berl)* 91: 95–102, 2013.
6. **Delima RD, Chua AC, Tirnitz-Parker JE, Gan EK, Croft KD, Graham RM, Olynyk JK, Trinder D.** Disruption of HFE and TFR2 causes iron-induced liver injury in mice. *Hepatology* 56: 585–593, 2012.
7. **Diez JJ, Iglesias P.** The role of the novel adipocyte-derived protein adiponectin in human disease: an update. *Mini Rev Med Chem* 10: 856–869, 2010.
8. **Dongiovanni P, Ruscica M, Rametta R, Recalcati S, Steffani L, Gatti S, Girelli D, Cairo G, Magni P, Fargion S, Valenti L.** Dietary iron overload induces visceral adipose tissue insulin resistance. *Am J Pathol* 182: 2254–2263, 2013.
9. **Fleming RE, Feng Q, Britton RS.** Knockout mouse models of iron homeostasis. *Annu Rev Nutr* 31: 117–137, 2011.
10. **Fleming RE, Ponka P.** Iron overload in human disease. *N Engl J Med* 366: 348–359, 2012.
11. **Gabrielsen JS, Gao Y, Simcox JA, Huang J, Thorup D, Jones D, Cooksey RC, Gabrielsen D, Adams TD, Hunt SC, Hopkins PN, Cefalu WT, McClain DA.** Adipocyte iron regulates adiponectin and insulin sensitivity. *J Clin Invest* 122: 3529–3540, 2012.
12. **Galaris D, Pantopoulos K.** Oxidative stress and iron homeostasis: mechanistic and health aspects. *Crit Rev Clin Lab Sci* 45: 1–23, 2008.
13. **Ganz T.** Systemic iron homeostasis. *Physiol Rev* 93: 1721–1741, 2013.
14. **George DK, Goldwurm S, MacDonald GA, Cowley LL, Walker NI, Ward PJ, Jazwinska EC, Powell LW.** Increased hepatic iron concentration in nonalcoholic steatohepatitis is associated with increased fibrosis. *Gastroenterology* 114: 311–318, 1998.
15. **Gkouvatsos K, Fillebeen C, Daba A, Wagner J, Sebastiani G, Pantopoulos K.** Iron-dependent regulation of hepcidin in Hjv−/− mice: Evidence that hemojuvelin is dispensable for sensing body iron levels. *PLoS ONE* 9: e85530, 2014.
16. **Graham RM, Chua AC, Carter KW, Delima RD, Johnstone D, Herbison CE, Firth MJ, O'Leary R, Milward EA, Olynyk JK, Trinder D.** Hepatic iron loading in mice increases cholesterol biosynthesis. *Hepatology* 52: 462–471, 2010.
17. **Huang FW, Pinkus JL, Pinkus GS, Fleming MD, Andrews NC.** A mouse model of juvenile hemochromatosis. *J Clin Invest* 115: 2187–2191, 2005.
18. **Huang J, Gabrielsen JS, Cooksey RC, Luo B, Boros LG, Jones DL, Jouihan HA, Soesanto Y, Knecht L, Hazel MW, Kushner JP, McClain DA.** Increased glucose disposal and AMP-dependent kinase signaling in a mouse model of hemochromatosis. *J Biol Chem* 282: 37501–37507, 2007.
19. **Imeryuz N, Tahan V, Sonsuz A, Eren F, Uraz S, Yuksel M, Akpulat S, Ozcelik D, Haklar G, Celikel C, Avsar E, Tozun N.** Iron preloading aggravates nutritional steatohepatitis in rats by increasing apoptotic cell death. *J Hepatol* 47: 851–859, 2007.
20. **Kirsch R, Sijtsema HP, Tlali M, Marais AD, Hall Pde L.** Effects of iron overload in a rat nutritional model of non-alcoholic fatty liver disease. *Liver Int* 26: 1258–1267, 2006.
21. **Li Z, Soloski MJ, Diehl AM.** Dietary factors alter hepatic innate immune system in mice with nonalcoholic fatty liver disease. *Hepatology* 42: 880–885, 2005.
22. **Meli R, Mattace Raso G, Irace C, Simeoli R, Di Pascale A, Paciello O, Pagano TB, Calignano A, Colonna A, Santamaria R.** High Fat Diet Induces Liver Steatosis and Early Dysregulation of Iron Metabolism in Rats. *PLoS ONE* 8: e66570, 2013.
23. **Nelson JE, Bhattacharya R, Lindor KD, Chalasani N, Raaka S, Heathcote EJ, Miskovsky E, Shaffer E, Rulyak SJ, Kowdley KV.** HFE C282Y mutations are associated with advanced hepatic fibrosis in Caucasians with nonalcoholic steatohepatitis. *Hepatology* 46: 723–729, 2007.
24. **Nelson JE, Klintworth H, Kowdley KV.** Iron metabolism in Nonalcoholic Fatty Liver Disease. *Curr Gastroenterol Rep* 14: 8–16, 2012.
25. **Nelson JE, Wilson L, Brunt EM, Yeh MM, Kleiner DE, Unalp-Arida A, Kowdley KV, and Nonalcoholic Steatohepatitis Clinical Research N.** Relationship between the pattern of hepatic iron deposition and histological severity in nonalcoholic fatty liver disease. *Hepatology* 53: 448–457, 2011.
26. **Otogawa K, Kinoshita K, Fujii H, Sakabe M, Shiga R, Nakatani K, Ikeda K, Nakajima Y, Ikura Y, Ueda M, Arakawa T, Hato F, Kawada N.** Erythrophagocytosis by liver macrophages (Kupffer cells) promotes oxidative stress, inflammation, and fibrosis in a rabbit model of steatohepatitis: implications for the pathogenesis of human nonalcoholic steatohepatitis. *Am J Pathol* 170: 967–980, 2007.
27. **Pantopoulos K.** Function of the hemochromatosis protein HFE: Lessons from animal models. *World J Gastroenterol* 14: 6893–6901, 2008.
28. **Papanikolaou G, Samuels ME, Ludwig EH, MacDonald ML, Franchini PL, Dube MP, Andres L, MacFarlane J, Sakellaropoulos N, Politou M, Nemeth E, Thompson J, Risler JK, Zaborowska C, Babakaiff R, Radomski CC, Pape TD, Davidas O, Christakis J, Brissot P, Lockitch G, Ganz T, Hayden MR, Goldberg YP.** Mutations in HFE2 cause iron overload in chromosome 1q-linked juvenile hemochromatosis. *Nat Genet* 36: 77–82, 2004.
29. **Pietrangelo A.** Hereditary hemochromatosis: pathogenesis, diagnosis, treatment. *Gastroenterology* 139: 393–408, 2010.
30. **Powell EE, Ali A, Clouston AD, Dixon JL, Lincoln DJ, Purdie DM, Fletcher LM, Powell LW, Jonsson JR.** Steatosis is a cofactor in liver injury in hemochromatosis. *Gastroenterology* 129: 1937–1943, 2005.
31. **Ramm GA, Ruddell RG.** Hepatotoxicity of iron overload: mechanisms of iron-induced hepatic fibrogenesis. *Semin Liver Dis* 25: 433–449, 2005.
32. **Rohrlich PS, Fazilleau N, Ginhoux F, Firat H, Michel F, Cochet M, Laham N, Roth MP, Pascolo S, Nato F, Coppin H, Charneau P, Danos O, Acuto O, Ehrlich R, Kanellopoulos J, Lemonnier FA.** Direct recognition by alphabeta cytolytic T cells of Hfe, a MHC class Ib molecule without antigen-presenting function. *Proc Natl Acad Sci USA* 102: 12855–12860, 2005.
33. **Sebastiani G, Gkouvatsos K, Maffettone C, Busatto G, Guido M, Pantopoulos K.** Accelerated CCl_4-induced liver fibrosis in Hjv−/− mice, associated with an oxidative burst and precocious profibrogenic gene expression. *PLoS ONE* 6: e25138, 2011.
34. **Sebastiani G, Pantopoulos K.** Disorders associated with systemic or local iron overload: from pathophysiology to clinical practice. *Metallomics* 3: 971–986, 2011.
35. **Shi Z, Wakil AE, Rockey DC.** Strain-specific differences in mouse hepatic wound healing are mediated by divergent T helper cytokine responses. *Proc Natl Acad Sci USA* 94: 10663–10668, 1997.
36. **Sonnweber T, Ress C, Nairz M, Theurl I, Schroll A, Murphy AT, Wroblewski V, Witcher DR, Moser P, Ebenbichler CF, Kaser S, Weiss G.** High-fat diet causes iron deficiency via hepcidin-independent reduction of duodenal iron absorption. *J Nutr Biochem* 23: 1600–1608, 2012.
37. **Sorrentino P, D'Angelo S, Ferbo U, Micheli P, Bracigliano A, Vecchione R.** Liver iron excess in patients with hepatocellular carcinoma developed on non-alcoholic steato-hepatitis. *J Hepatol* 50: 351–357, 2009.
38. **Tan TC, Crawford DH, Jaskowski LA, Murphy TM, Heritage ML, Subramaniam VN, Clouston AD, Anderson GJ, Fletcher LM.** Altered

lipid metabolism in Hfe-knockout mice promotes severe NAFLD and early fibrosis. *Am J Physiol Gastrointest Liver Physiol* 301: G865–G876, 2011.

39. **Valenti L, Fracanzani AL, Bugianesi E, Dongiovanni P, Galmozzi E, Vanni E, Canavesi E, Lattuada E, Roviaro G, Marchesini G, Fargion S.** HFE genotype, parenchymal iron accumulation, and liver fibrosis in patients with nonalcoholic fatty liver disease. *Gastroenterology* 138: 905–912, 2010.
40. **Wang J, Pantopoulos K.** Regulation of cellular iron metabolism. *Biochem J* 434: 365–381, 2011.